crystals

MDPI

Article

Influence of Polymer Latexes on the Properties of High Performance Cement–Based Materials

Daxiang Cheng [1], Xiaosheng Li [1,2], Xu Gao [1,*], Xiaochun Fan [1], Rui Zhao [1] and Tingli Yang [1]

[1] School of Civil Engineering and Architecture, Wuhan University of Technology, Wuhan 430070, China; chengdxdr@163.com (D.C.); xiao-sheng.li@polyu.edu.hk (X.L.); fxcfree@126.com (X.F.); zhaoruiwork2022@163.com (R.Z.); yang225603@163.com (T.Y.)

[2] Department of Civil and Environmental Engineering, The Hong Kong Polytechnic University, Hong Kong, China

* Correspondence: x.gao@whut.edu.cn; Tel.: +86-177-0276-8017

Abstract: The application of polymer latex provides an additional approach when optimizing the properties of high–performance cement–based materials. Given that cement–based materials are extraordinarily sensitive to the characteristics and relative content of polymer latexes, identifying their influence is essential for application. This paper investigates the impact of polymer latex types and its relative content on the mechanical properties, hydration product, pore structure, and drying shrinkage of cement–based materials with a low water to binder ratio. The results showed that the mechanical properties, pore structure, and drying shrinkage of the styrene butadiene latex modified samples were better than those of ethylene vinyl acetate latex and silicone acrylic latex modified ones. Incremental increases to the polymer to cement ratio induces a slight reduction on compressive strength, and styrene–butadiene latex promotes tensile strength. Polymer latex hinders the transformation from ettringite to monosulfate, reducing the bound water and portlandite generated. Increasing the polymer content induces more significant stretching in the vibration peak of SO_4 from ettringite. Further incorporation of polymer latex contributes to ettringite precipitation and the decline of harmful pores. Polymer addition also results in lower drying shrinkage compared with the reference group.

Keywords: polymer latex; low water–binder ratio; mechanical properties; hydration products; drying shrinkage

Citation: Cheng, D.; Li, X.; Gao, X.; Fan, X.; Zhao, R.; Yang, T. Influence of Polymer Latexes on the Properties of High Performance Cement–Based Materials. *Crystals* **2022**, *12*, 789. https://doi.org/10.3390/cryst12060789

Academic Editor: Tomasz Sadowski

Received: 22 April 2022
Accepted: 27 May 2022
Published: 30 May 2022

1. Introduction

Polymer latex modified cement–based materials are composites prepared by incorporating organic polymer compounds into Portland cement mixes [1]. After mixing, the polymer particles are evenly distributed in the cement slurry, and they experience a series of physicochemical reactions, including film–forming, complexation, flocculation, and so on [2]. The main modification mechanisms of polymer latex on cement–based materials are adsorption, complexation, and film–forming [3–7]. These interactions between cement and polymer particles redefine the microstructure and interface characteristics of traditional cement–based materials, thus contributing to the improvement of flexural properties and durability at the macro level [8]. With the fast development of modern infrastructure construction, high–performance concrete characterized by a relatively low water to binder ratio is widely employed, but it is also accompanied by large shrinkage and flexural properties [9,10]. The application of polymer latex might pave the way for the optimal design of high–performance cement–based materials.

Tsigarida et al. studied the effect of material surface roughness on the durability of samples and believed that the hydrophobicity of samples treated with polymer latex was greatly improved, which was helpful for improving the durability of samples [11,12].

Rottstegge et al. reveals that the addition of polymer latex increases the ettringite generated. Polymer latex also contributes to a weak network structure with hydration products which improves the mechanical properties correspondingly [13]. Shi et al. investigates the potential modification of styrene–butadiene and silicone–acrylic latex on the microcosmic mechanism of the toughness; it was suggested that the formation of continuous polymer film structures in the cement–based material system determines the effect of modification [14]. Knapen et al. believe that polymers contribute to better dispersion of cement particles and more sufficient cement hydration [15]. Kong et al. explore the retarding effect of styrene acrylic latex on cement hydration and find that polymer employment delays heat release during cement hydration [16]. Ohama et al. incorporate styrene–butadiene and polyethylene vinyl acetate latexes into the cementitious system, discovering that the film formation from the polymer decreases the shrinkage performance of matrix [17]. Sowoidnich et al. clarify the slight water–reducing effect of the polymer in a cement–based system and claim that polymer latex has better prospects under a low water to binder ratio [18]. The type and dosage of polymer are the most critical factors that influence high performance cement–based materials [19,20]; therefore, exploring the feasibility of the polymer under a low water–binder ratio, and the performance characteristics of organic–inorganic cement–based composites, possess much practical significance.

In this study, the feasibility and potential modifications of polymer latex on high performance cement–based materials are conducted. The macro and microscopic properties of polymer modified cement–based materials with a low water to binder ratio are investigated. Styrene–butadiene, ethylene–vinyl acetate copolymer, and silicone–acrylic latex are selected. The potential effects of latex type and relative content on the mechanical properties, hydration products, and dry shrinkage process are evaluated.

2. Materials and Methods

2.1. Materials

Commercial P.I 42.5 Portland cement is used in this study as the binder. The main chemical components of the Portland cement is listed in Table 1. The styrene–butadiene latex (SBR), ethylene–vinyl acetate copolymer latex (EVA), and silicone–acrylic latex (SAE) used in this study are industrial grade polymer latexes. The minimum film forming temperatures of three types of polymer latexes are 15 °C, 0 °C, and 24 °C, respectively. The solid contents are 48%, 54.5% and 48%, respectively. The characteristic parameters of polymer latex are provided by the manufacturer and listed in Table 2.

Table 1. Portland cement main chemical composition (wt. %).

SiO_2	Al_2O_3	CaO	MgO	Fe_2O_3	Na_2O	f–CaO	SO_3
20.95	5.19	64.29	1.85	3.83	0.52	0.96	0.95

Table 2. Characteristic parameters of polymer latex.

Types	pH	PS (μm)	MFT * (°C)	SC (%)	V (map·s)
SBR	7.0–9.0	0.112	15	48	50–150
EVA	9.6	2	0	54.5	2206
SAE	7.0–8.0	2	24	48	1000–3000

* MFT—minimum film forming temperature.

The fine aggregate used in this study is GB/T 14684–2001 standard sand. Polycarboxylic superplasticizer with solid content of 14% is used as plasticizer.

2.2. Mix Proportioning and Paste/Mortar Preparation

In this experiment, 16 groups of standard mortar samples were designed, the reference dosage of Portland cement is 450 g, the water–binder ratio is fixed at 0.22, the sand/cement ratio is fixed at 3:1, and the plasticizer dosage is 1.7%. The three types of polymer latexes

used in the experiment are called SBR, EVA, and SAE. The polymer–cement ratio is set at five gradients of 3%, 6%, 9%, 12% and 15% of the cement mass, numbered 1–5.

The mixing procedures for paste and mortar are conducted based on the GB/T 17,671 standard. Samples were prepared using a planetary paste/mortar mixer and the solid materials were added into the mixer followed by mixing water. The fresh paste was poured into plastic molds of 40 × 40 × 40 mm^3 and 40 × 40 × 160 mm^3 after mixing, then covered with a plastic film on the top surface for 24 h. The formed paste and mortar samples are shown in Figure 1.

(**a**) (**b**)

Figure 1. Formed sample: (**a**) mortar sample; (**b**) paste sample.

After the sample is prepared, it is placed in the standard curing room with a temperature of (20 ± 2) °C and relative humidity of 95% for 7 days, and then moved to a room with a temperature of (20 ± 2) °C until it is cured for 28 days. Table 3 shows the sample mix proportion.

Table 3. Mix proportions.

Sample ID	P/C	W/C	Sp/C
Reference	0%	0.22	1.7%
SBR1–5	3%, 6%, 9%, 12%, 15%	0.22	1.7%
EVA1–5	3%, 6%, 9%, 12%, 15%	0.22	1.7%
SAE1–5	3%, 6%, 9%, 12%, 15%	0.22	1.7%

2.3. Methods

The mechanical properties are tested in accordance with "GB/T 17671–1999 Test method for strength of cement mortar". The loading rate is set at 2.4 kN/s.

The crystalline phase composition of the hydration products is characterized by X–ray diffraction with 2θ scope of 5–50° and a scanning rate of 2°/min. The empyrean diffractometer used is from Panalytical, the Netherlands.

The phase composition of hydration products is characterized by a simultaneous thermal analyzer with a test temperature range of 40–1000 °C and a heating rate of 10 °C/min. The STA449F3 simultaneous thermal analyzer used is from Netzsch instruments, Germany.

The functional groups of hydration products are tested with a Fourier transform infrared spectrometer. FTIR spectra are taken in a Nexus spectrometer. The nexus spectrometer used is from Thermo Nicolet Corporation in the United States. Powdered samples are mixed with KBr and pressed into pellets. The analysis frequency range of the sample is 4000~400 cm^{-1} with a 4.0 resolution and 128 scans.

The pore structure of the hardened cement matrix is tested by mercury intrusion porosimetry. The auto Auto Pore IV 9510 mercury porosimeter of the Micromeritics com-

pany of the United States is used. The equilibrium time of high and low pressure is 10 s, the emptying time is 5 min, and the pore diameter measurement range is 3~35 μm.

The drying shrinkage performance is tested with a vertical mortar shrinkage meter. The drying shrinkage rate *St* (%) is calculated by the ratio of the difference between the initial length of the specimen and the length at each age to the effective length of the specimen minus the length of the metal probes on both sides. BC-176 vertical mortar shrinkage meter used is from Henan Keyu company, China.

Among the abovementioned tests, the strength and the drying shrinkage results of each mix was obtained from the average of three specimens, and one sample was used for MIP, XRD, TG–DTG, FTIR tests.

3. Results and Discussion

3.1. Mechanical Properties

Figure 2 shows the effect of polymer latex on the mechanical properties of polymer latex. On one hand, the compressive strengths of the reference group at 3 days, 7 days, and 28 days are 59.4 MPa, 63.1 MPa, and 80.8 MPa. The compressive strength of EVA latex modified samples at each curing age decrease linearly with an increase in the polymer–cement ratio. The compressive strength of SBR latex modified samples show the trend of decreasing after rising. The compressive strength of the SAE latex modified samples exhibits a similar tendency. The optimum dosage of polymer latex is 6% of the polymer–cement ratio. When the polymer–cement ratio is increased to 15%, the 28 day compressive strength of SBR–5, EVA–5, and SAE–5 is 49.9 MPa, 46.6 MPa, and 47.6 MPa, respectively, which is 38.2%, 42.3%, and 41.1% lower than that of the reference group. It is indicated that the dosage of polymer latex is not too large at a low water–binder ratio. Otherwise, the compressive strength will be significantly reduced. Under the same polymer–cement ratio, the effects of three kinds of polymer latex on compressive strength are compared. When the polymer–cement ratio is 3%, the EVA latex modified sample achieves the optimal compressive strength. Under other polymer to cement ratios, the SBR latex modified samples exhibits the highest compressive strength. It shows that the negative effect of SBR latex on the compressive strength is lower than that of the other two latexes, which may be caused by the smaller viscosity of SBR latex and less air entrainment during stirring. On the other hand, the amount of carboxyl groups on the surface of SBR latex is less than that of ethylene vinyl acetate and silicone acrylic latexes. In the process of cement hydration, the adsorption capacity of SBR latex is low, and the hindering effect of cement hydration is not significant, resulting in the best compressive strength of SBR latex modified samples [21].

On the other hand, the flexural strengths of the reference group at 3 days, 7 days, and 28-days are 7.5 MPa, 8.2 MPa, and 9.0 MPa, respectively. For SBR latex modified samples, the flexural strength of each curing age shows a gradual improvement with an increase in the polymer–cement ratio. For EVA latex modified samples, the flexural strength shows a trend of increase before decline with the further incorporation of the polymer–cement ratio; however, all of them are lower than those of the reference group. For SAE latex modified samples, the flexural strength of each curing age shows an approximate linear decline with an increase in the polymer–cement ratio. The effects of the three polymer latexes on the flexural strength are compared under the same polymer–cement ratio. Moreover, it is discovered that when the polymer–cement ratio is 3%, the SAE latex–modified sample achieves the best flexural strength. The flexural strengths of the SBR latex–modified samples are best under other polymer–cement ratio gradients. It shows that SBR latex exhibits a limited negative impact on compressive strength, but it contributes to the improvement of flexural strength to some extent. This may be due to the fact that the polymer latex could form a three–dimensional network structure that penetrates itself with the hydration products after drying. When the sample undergoes flexural failure, microcracks appear; however, the concentrated stress at the microcracks can be dispersed through the polymer latex films, thus improving the flexural properties of the hardened cement matrix [22].

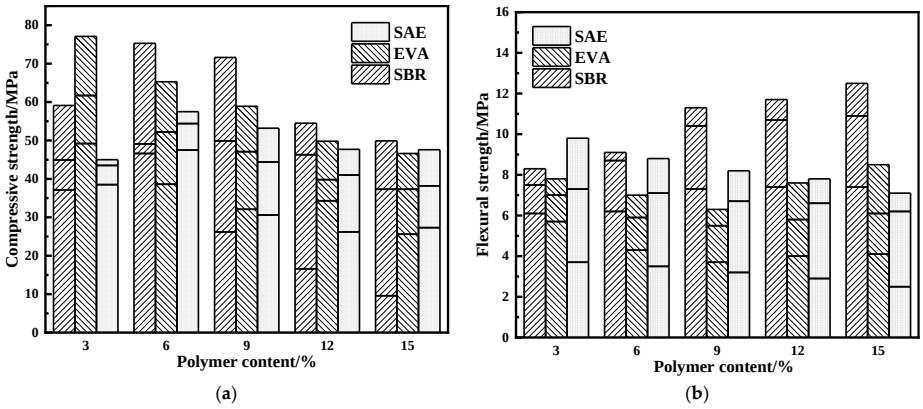

Figure 2. Effect of polymer latex content and type on compressive/flexural strength of mortar samples: (**a**) compressive strength; (**b**) flexural strength.

3.2. Shrinkage Properties

Drying shrinkage of polymer modified cement–based materials usually refers to the situation wherein the cement–based materials stop curing, the system gradually loses free water, and the pore pressure increases under the condition of natural drying, resulting in volume reduction. Figure 3 shows the effect of polymer latexes on the shrinkage properties of cement–based materials. It can be seen from the figure that the drying shrinkage rate of the reference group after curing for 28 days is 0.068%. At the same time, when the samples are cured for 28 days, the drying shrinkage rates of SBR–2 and SBR–4 are 0.038% and 0.034%. Moreover, the drying shrinkage rates of EVA–2 and EVA–4 are 0.047% and 0.043%. The drying shrinkage rates of SAE–2 and SAE–4 account for 0.041% and 0.036%, respectively. The comparison shows that the drying shrinkage of polymer latex modified samples is significantly lower than that of the reference group, and each curve exhibits a consistent trend with the increase on the polymer content, which increases rapidly during the early stage and gradually flattens in the later stage. When the relative content of polymer latex changes, the drying shrinkage of polymer latex modified samples decreases with the increase of the polymer–cement ratio. In addition, the decreasing effects of polymer latex types on drying shrinkage are SBR, SAE, and EVA, which may be related to the different air–entraining and film–forming effects of different polymer latexes.

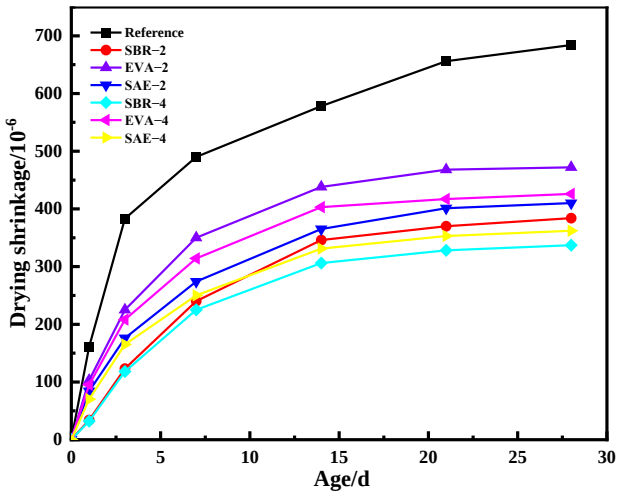

Figure 3. Effect of polymer latex content and type on drying shrinkage of mortar samples.

3.3. Pore Structure Analysis

Figure 4 demonstrates the test results of the total porosity and characteristic pore parameters of each modified sample after curing for 28 days by mercury intrusion porosimetry.

It can be seen that the total porosity of the reference group is 0.18 mL/g, and the total porosity of the other polymer latex modified samples is greater than that of the reference group, indicating that the addition of polymer latex increases the total porosity of the system. Except for the styrene–butadiene latex modified samples, the total porosity of the other samples increases with the amount of polymer latex content. On the other hand, the type of polymer latex also exhibits an effect on the total porosity of the hardened cement matrix. The total porosity of SBR–4 was 0.23 mL/g, whereas the total porosity of EVA–4 was 0.27 mL/g, and the total porosity of SAE–4 increased to 0.28 mL/g. This phenomenon shows that the air entrainment amount of the silicone–acrylic latex modification is higher than that of the other two latexes, which, in turn, leads to a decrease in the compactness of the specimen. This explains why the mechanical properties of the SAE latex–modified specimen decrease the most significantly, as mentioned above.

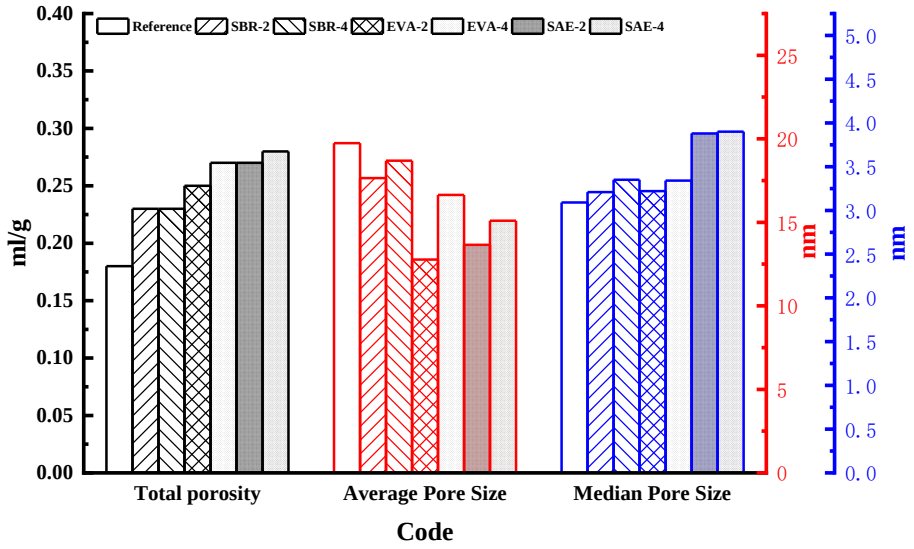

Figure 4. Porosity and characteristic porosity parameters of paste samples at 28 days.

According to the effect on shrinkage deformation, the pores in the hardened cement matrix can be divided into [23]: large pores with a pore size of >50 nm, fine pores with a pore diameter of 50–10 nm, and gel pores of 10 nm. The average pore size and median pore size of the hardened cement matrix increases as the polymer latex content increases. It is suggested that the film formation and flocculation of the polymer latex could optimize the microscopic pore structure in the system, thus increasing the number of harmless pores in the system and filling the large capillary pores and fine capillary pores of the cement paste. Pore refinement reduces the amount of evaporable water and makes the migration of moisture difficult, thereby reducing the total shrinkage and slowing the development of drying shrinkage. Due to the air–entraining effect of the polymer latex, the total porosity of the modified sample is larger than that of the reference group, and cracks are more likely to develop during the stress process, thus affecting the compressive strength of the modified sample. The change of the flexural strength with the pore structure shows that the film–forming, filling, and sealing effects of the polymer not only improve the pore shape, but also reduce the orientation of the crystals inside the material, and the network structure formed by the polymer and the cement hydration product is more dense. In addition, the polymer has a "bridging" effect in the cement stone, resulting in a significantly improved flexibility of the modified material compared with the unmodified material, and an increase in the flexural strength at the macro level.

3.4. X-ray Diffraction Analysis

Figure 5 depicts the XRD patterns of the groups with polymer–cement ratios of 0%, 6% and 12% at 28 days. It is revealed that the main mineral phases after 28 days of hydration are dehydrated C_3S and C_2S from cement clinker, ettringite, portlandite, and tetracalcium ferrite [24,25]. The diffraction pattern of the modified and reference groups exhibits limited differences. The above phenomena illustrate that the polymer latex that possibly induced complexation or film formation cannot significantly influence the types of hydration products [26]. It should be noted that the diffraction peak intensities of C_3S and C_2S demonstrate insignificant changes under different polymer latexes.

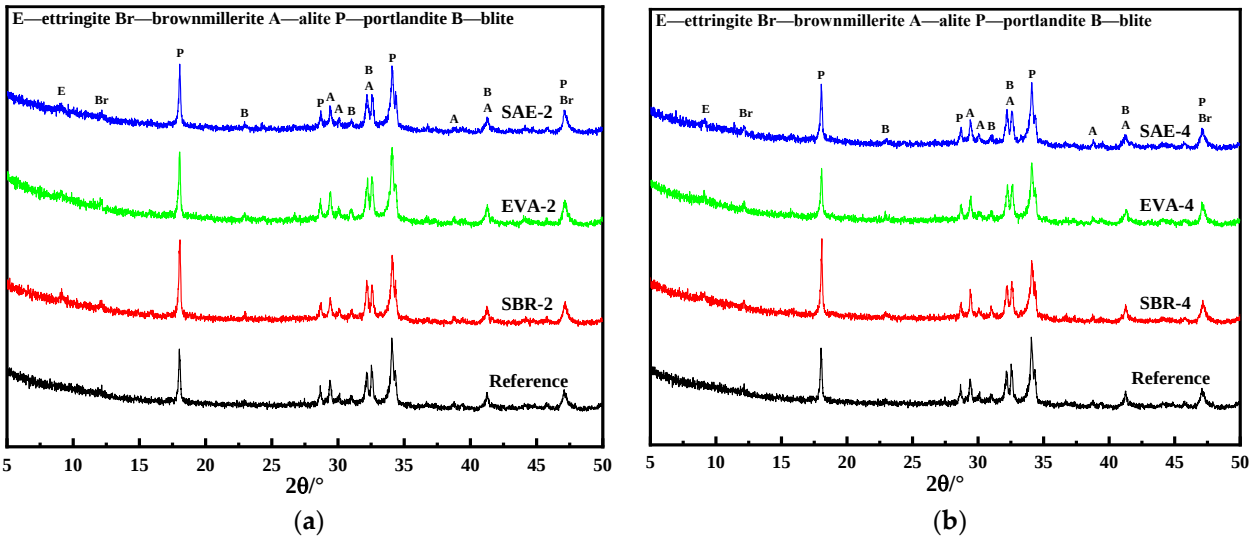

Figure 5. XRD patterns of paste samples with different types and contents of polymer latex at 28 days: (**a**) polymer–cement ratio is 6%; (**b**) polymer–cement ratio is 12%.

By comparing the XRD patterns of the reference and testing groups, it is demonstrated that the incorporation of polymer latex induces a stronger diffraction peak of portlandite. When the polymer–cement ratio is fixed, the diffraction peak intensity of the portlandite with EVA latex added is relatively weaker. Moreover, the intensity of portlandite is negatively correlated with the additional amount of EVA latex. The results are consistent with the literature [27]. This should be attributed to the reduced portlandite precipitation induced by complexation of the carboxyl groups on the surface of EVA latex particles.

3.5. Simultaneous Thermal Analysis

Figure 6 reveals the TG curve of the sample at 28 days of curing. Before 200 °C, the weight loss of the sample is mainly caused by C–S–H dehydration and Ettringite decomposition [28,29]. The TG curve of each sample in the figure exhibits limited differences before 200 °C, indicating that the influence of the polymer latex incorporation system on low–temperature decomposition products is relatively limited. For the same polymer latex, the increased polymer–cement ratio results in improvement in weight loss from 400 °C to 500 °C. With the increase in the amount of polymer latex, the weight loss of the hardened cement matrix before 1000 °C also increases. Compared with the reference group, the weight loss of SBR–2, EVA–2, and SAE–2 increased by 3.76%, 1.90% and 2.69%, and the weight loss of SBR–4, EVA–4, and SAE–4 increased by 6.98%, 4.76% and 5.53%. For different polymer latexes, the weight loss of the samples in SBR, SAE, and EVA decreases gradually.

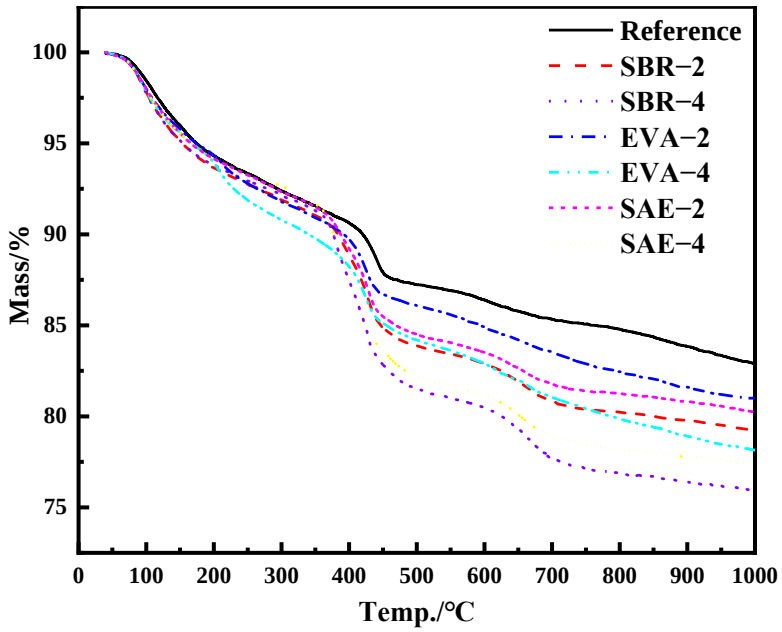

Figure 6. TG diagram of paste samples with different polymer latex types and contents at 28 days.

Figure 7 reveals the DTG curve of the sample at 28 days of curing. The weight loss peak of C–S–H gel decomposition is around 100 °C, the weight loss temperature of ettringite is in the range of 50–160 °C, peaking at around 100 °C. The partial weight loss temperature of monosulfate is in the range of 130–220 °C, and the peak value is around 170 °C. The portlandite decomposition peak is around 425 °C, and the carbonate decomposition peak is around 670 °C [28–30]. In the DTG curve, the ettringite decomposition peak area of the polymer latex modified sample is significantly higher than that of the reference group. Moreover, the area for the portlandite decomposition peak of the polymer latex modified sample is also higher than that of the reference group. In addition, the special peaks at around 210 °C are decomposition peaks from the ethylene–vinyl acetate copolymer latex. The special peaks at about 385 °C are the styrene–butadiene latex and silicone–acrylic latex decomposition peaks. The incorporation of polymer latex hinders the transformation from ettringite to monosulfate in cement hydration products. It is obvious from the DTG curve that only the reference group exhibits the monosulfate decomposition peak, which is consistent with other literature reports [23]. In addition, the weight loss peaks of the polymer latex modified samples around 670 °C are higher than those of the reference group. This phenomenon is due to the fact that the polymer latex, or its decomposition products, can interact with dehydrated cement particles or hydration products when the polymer is heated, leading to the formation of carbonate or carbonate–like phases [31].

Quantitative methods are used to calculate the amount of chemically bound water and $Ca(OH)_2$ in the hardened cement matrix to further investigate the effect of polymer latex on hydration products. It should be noted that in light of the thermal decomposition of the polymer latex, the calculation result of the amount of bound water is too large, so in the calculation concerning polymer latex, induced weight loss is excluded when calculating the amount of bound water and calcium hydroxide content [15]. The specific calculation method is shown in Formula (1):

$$H[\%] = \frac{m_{40^\circ C}(1 - L_{cem}) - m_{1000^\circ C}\left(1 + \frac{P}{C}L_{pol}\right)}{m_{1000^\circ C}\left(1 - \frac{P}{C}\left(1 - L_{pol}\right)\right)} \quad (1)$$

where P/C is the mass ratio of polymer to cement, L_{cem} is the loss on ignition of cement, and L_{pol} is the loss on ignition of polymer latex.

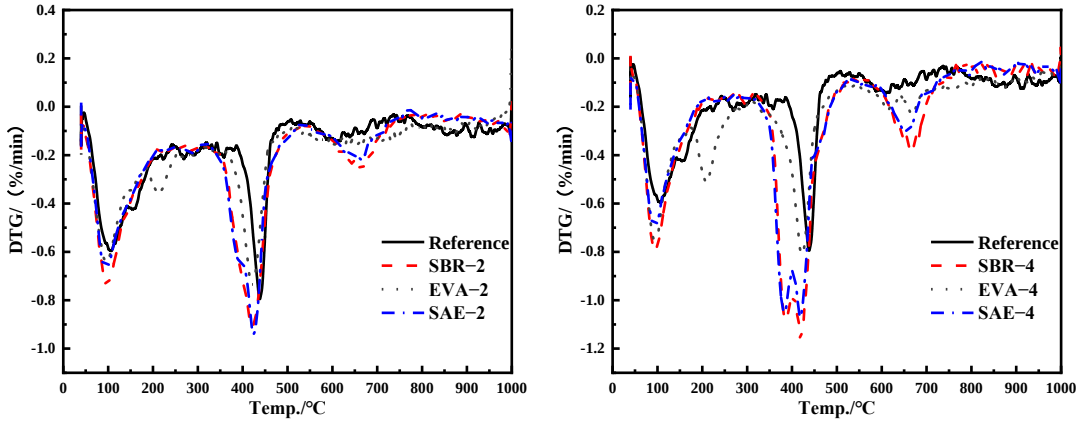

Figure 7. DTG curves of paste samples with different polymer latex types and contents at 28 days: (**a**) polymer–cement ratio is 6%; (**b**) polymer–cement ratio is 12%.

The calculation method of $Ca(OH)_2$ content is shown in Formula 2, where Δm is the thermogravimetric loss in the calculation temperature range; m is the initial mass; M_{CH} is the molar mass of $Ca(OH)_2$; M_{loss} is the molar mass of water.

$$CH[\%] = \frac{\Delta m}{m} \times \frac{M_{CH}}{M_{loss}} \times 100\% \quad (2)$$

The calculation results are shown in Table 4. After 28 days of hydration, the bound water content of the polymer–modified samples is lower than that of the reference group. Except for the ethylene vinyl acetate modified samples, the $Ca(OH)_2$ in the other samples' content is higher. Since the degree of cement hydration demonstrates a high correlation with the portlandite content, it can be inferred that the polymer latex affects the hydration of cement–based materials. Under the premise that the gypsum is consumed, the hydration product ettringite will react with calcium aluminate hydrate and portlandite to transform into the monosulfate, and the polymer latex hinders this process, resulting in a relative increase in the *CH* content.

Table 4. Influence of polymer latex on amount of bound water and portlandite content in hydration products.

Title	Reference	SBR–2	SBR–4	EVA–2	EVA–4	SAE–2	SAE–4
H_2O	20.7%	20.35%	19.2%	17.8%	17.9%	19.4%	20.1%
$Ca(OH)_2$	14.0%	18.7%	20.8%	13.8%	14.3%	17.8%	19.3%

3.6. FTIR Analysis

Figure 8 demonstrates the infrared spectrum of the hardened matrix of all groups. The peak near 970 cm^{-1} represents the stretching vibration of Si–O in Q_2 tetrahedron. With the further incorporation of the polymer latex, the peak frequency and polymerization degree of C–S–H display limited differences [32]. The peaks near 1417 cm^{-1} and 1470 cm^{-1} are the stretching vibration peaks of C–O, indicating the formation of carbides. For the reference group, the band near 1640 cm^{-1} is the bending vibration of H–O–H in water, and the band near 3430 cm^{-1} is the stretching vibration of H–O–H. With the further addition of the polymer latex, the position belonging to stretching the vibration peak of water molecules shifts to a lower frequency. More specifically, the position of the stretching vibration peak in groups with SBR is even significantly reduced to 3441 cm^{-1}. Although the position attributed to the bending vibration peak of water molecules transfers to a higher frequency, the position of the bending vibration peak for samples with EVA remarkably increases to 1570 cm^{-1}. This is because the introduction of polymer latex changes the

environment around water molecules and the strength of hydrogen bond between water molecules, resulting in the variation of vibration frequencies in water molecules. The peak of 1733 cm^{-1} is the stretching vibration caused by a carbonyl group in SBR latex and SAE latex. The peak at 2970 cm^{-1} originates from the stretching vibration of –OH in the carboxyl group. The intensity of these two carboxyl group induced vibrations is positively correlated with the polymer–cement ratio. The peak located at about 3643 cm^{-1} is attributed to the O–H vibration in portlandite. The peak at about 3430 cm^{-1} is the stretching vibration of H–O–H from water, and the peak at about 1117 cm^{-1} results from the stretching vibration of SO_4 in ettringite [13]. With the addition of the polymer, the characteristic peak of ettringite becomes even more obvious, indicating that polymer latex contributes to ettringite precipitation during hydration.

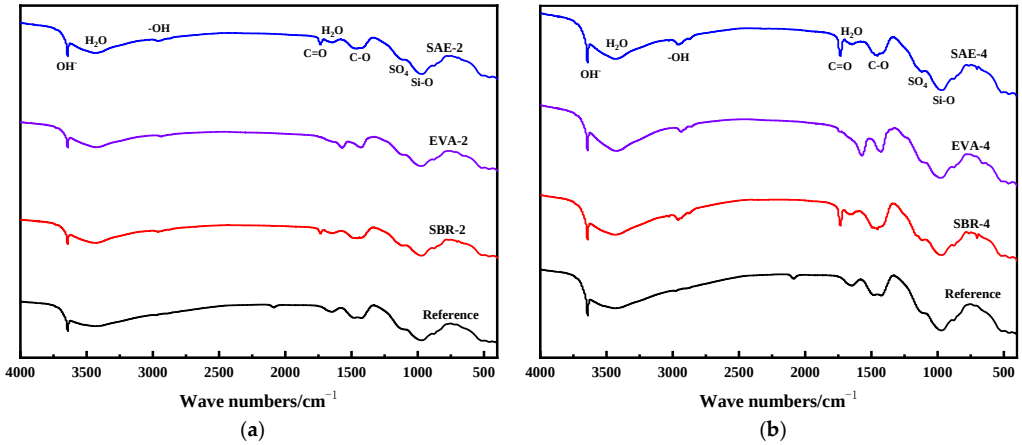

Figure 8. FTIR curves of paste samples with different polymer latex types and contents at 28 days: (**a**) polymer–cement ratio is 6%; (**b**) polymer–cement ratio is 12%.

In this study, the effects of the type and relative content of polymer latexes on the mechanical properties, hydration products, pore structure, and dry shrinkage process of cement–based materials were analyzed; however, because the polymer changes the hydration process of cement and the composition of hydration products, and its thermal decomposition temperature is similar to that of hydration products, it will interfere with the test of cement hydration degree in a variety of test methods, so the test results are a deviation.

4. Conclusions

In this study, the macro properties and microstructure of high–performance cementitious materials modified with three polymer latexes are investigated. The following conclusions can be drawn:

(1) The incorporation of a polymer latex induces a stronger diffraction peak of portlandite. With the increase of the relative content of the polymer latex, the weight loss of the modified samples increased; the weight loss of SBR–4 was 6.98% higher than that of the reference group. Polymer latexes retard conversion from ettringite to monosulfate, accompanied by the decline of the chemically bound water and promotion in portlandite. The relatively stronger stretching–vibration peak of SO_4 in ettringite proves the stability of ettringite. In addition, polymer latex also changes the hydrogen bond strength between water molecules, resulting in the change of vibration frequency of water molecules.

(2) Polymer latexes induce higher porosity with the average pore size reduced. The total porosity of the reference group was 0.18 mL/g. The total porosity of SBR–4 was 0.23 mL/g, whereas the total porosity of EVA–4 was 0.27 mL/g, and the total porosity of SAE–4 increased to 0.28 mL/g. The significance of polymer latexes on porosity exhibits the decreasing order of styrene–butadiene latex, ethylene vinyl

acetate copolymer, and silicone acrylate latex. Polymer latexes remarkably hinder drying shrinkage development owing to its water retention effect.

(3) Polymer latexes have no significant effect on the development of compressive strength. Although ethylene vinyl acetate copolymer and silicone acrylate latexes reduce the tensile strength, the tensile strength of the styrene–butadiene latex–modified samples is significantly improved. Styrene–butadiene latex increases the flexural strength at 28 days by 50% compared with reference group of 9.0 MPa.

Author Contributions: Literature search, D.C., R.Z. and T.Y.; study design, D.C., X.L., X.F. and X.G.; figure, data collection, D.C., R.Z. and T.Y.; data analysis, D.C. and X.L.; writing—D.C., X.L. and X.G. All authors have read and agreed to the published version of the manuscript.

Funding: The research has been financially supported by the National Science Foundation of China (No. 52178249).

Institutional Review Board Statement: Not applicable.

Informed Consent Statement: Not applicable.

Data Availability Statement: Not applicable.

Acknowledgments: The authors would like to acknowledge assistance from Lizhe Song, Rui Zhao, Xiaosheng Li and Tingli Yang from Wuhan University of Technology. Thanks to the State Key Laboratory of Silicate Materials for Architectures for providing the equipment.

Conflicts of Interest: The authors declare no conflict of interest.

Nomenclature

Symbol	Description	Units
C	Quality of P.I 42.5 Portland cement	g
CH	Content of $Ca(OH)_2$ in hydration products	%
DTG	Differential thermal gravity	
EVA	Ethylene–vinyl acetate copolymer latex	
FTIR	Fourier transform infrared reflection	
H	Content of bound water in hydration products	%
L_{cem}	The loss on ignition of cement	%
L_{pol}	The loss on ignition of polymer latex	%
m	Initial mass of sample	mg
Δm	The thermogravimetric loss in the calculation temperature range	mg
$m_{40^\circ C}$	Mass of sample at 40 °C	mg
$m_{1000^\circ C}$	Mass of sample at 1000 °C	mg
M_{CH}	The molar mass of $Ca(OH)_2$	g/mol
M_{loss}	The molar mass of water	g/mol
MFT	Minimum film forming temperature of polymer latex	°C
P	Quality of polymer latex	g
pH	The expression of acidity and alkalinity of aqueous solution	
PS	Particle size of polymer latex	μm
SAE	Silicone–acrylic latex	
SBR	Styrene–butadiene latex	
SC	Mass percentage of the remaining part of the polymer latex in the total amount after drying under the specified conditions	%
Sp	Quality of Superplasticizer	g
St	The physical quantity of volume or length reduction degree caused by drying and water loss of the sample	%
TG	Thermal Gravity Analysis	
V	Resistance of polymer latex to flow	map·s
W	Quality of Water	g

References

1. Satish, C.; Yoshihiko, O. *Polymers in Concrete*; CRC Press: Boca Raton, FL, USA, 2020; Volume 8, p. 12.
2. Ohama, Y. Recent progress in concrete–polymer composites. *Adv. Cem. Based Mater.* **1997**, *5*, 31–40. [CrossRef]
3. Renuka, S.M.; Suraj, R.; Siva, A.; Mugahed, A.; Radhamanohar, A.; Nikolai, V.; Roman, F. The Effect of Superabsorbent Polymer and Nano–Silica on the Properties of Blended Cement. *Crystals* **2021**, *11*, 1394.
4. He, Y.H.; Mo, L.W.; Mao, Z.Y.; Huang, F.F.; Han, Z.H. Influence of Polyvinyl Alcohol Powder on the Mechanical Performance and Volume Stability of Sulfoaluminate–Portland Cement Composite. *Crystals* **2021**, *11*, 692. [CrossRef]
5. Guo, S.Y.; Zhang, X.; Chen, J.Z.; Mou, B.; Ren, J. Mechanical and interface bonding properties of epoxy resin reinforced Portland cement repairing mortar. *Constr. Build. Mater.* **2020**, *264*, 120715. [CrossRef]
6. Bahranifard, Z.; Tabrizi, F.F.; Vosoughi, A.R. An investigation on the effect of styrene–butyl acrylate copolymer latex to improve the properties of polymer modified concrete. *Constr. Build. Mater.* **2019**, *205*, 175–185. [CrossRef]
7. Bessaies, B.H.; Baumann, R.; Schmitz, M.; Radler, M.; Roussel, N. Effect of polyacrylamide on rheology of fresh cement pastes. *Cem. Concr. Res.* **2015**, *76*, 98–106. [CrossRef]
8. Zhang, X.J.; Du, M.R.; Fang, H.Y.; Shi, M.S.; Zhang, C.; Wang, F.M. Polymer–modified cement mortars: Their enhanced properties, applications, prospects, and challenges. *Constr. Build. Mater.* **2021**, *299*, 124290. [CrossRef]
9. Chen, X.; Yuan, J.; Dong, Q.; Zhao, X. Meso–scale cracking behavior of Cement Treated Base material. *Constr. Build. Mater.* **2020**, *239*, 117823. [CrossRef]
10. Maruyama, I.; Teramoto, A. Temperature dependence of autogenous shrinkage of silica fume cement pastes with a very low water–binder ratio. *Cem. Concr. Res.* **2013**, *50*, 41–50. [CrossRef]
11. Tsigarida, A.; Tsampali, E.; Konstantinidis, A.A.; Stefanidou, M. On the Use of Confocal Microscopy for Calculating the Surface Microroughness and the Respective Hydrophobic Properties of Marble Specimens. *J. Build. Eng.* **2021**, *33*, 101876. [CrossRef]
12. Macek, W. Fracture Surface Formation of Notched 2017A–T4 Aluminium Alloy under Bending Fatigue. *Int. J. Fract.* **2021**, *934*, 1–17. [CrossRef]
13. Rottstegge, J.; Arnold, M.; Herschke, L.; Glasser, G. Solid state NMR and LVSEM studies on the hardening of latex modified tile mortar systems. *Cem. Concr. Res.* **2005**, *35*, 2233–2243. [CrossRef]
14. Shi, C.; Zou, X.W.; Yang, L.; Wang, P.; Niu, M.D. Influence of humidity on the mechanical properties of polymer–modified cement–based repair materials. *Constr. Build. Mater.* **2020**, *261*, 119928. [CrossRef]
15. Knapen, E.; Gemert, D.V. Cement hydration and microstructure formation in the presence of water–soluble polymers. *Cem. Concr. Res.* **2009**, *39*, 6–13. [CrossRef]
16. Kong, X.M.; Emmerling, S.; Pakusch, J.; Rueckel, M.; Nieberle, J. Retardation effect of styrene–acrylate copolymer latexes on cement hydration. *Cem. Concr. Res.* **2015**, *75*, 23–41. [CrossRef]
17. Ohama, Y.; Kan, S. Effects of specimen size on strength and drying shrinkage of polymer–modified concrete. *Int. J. Cem. Compos. Lightweight Concr.* **1982**, *4*, 229–233. [CrossRef]
18. Sowoidnich, T.; Rachowski, T.; RößLER, C.; Völkel, A.; Ludwig, H.M. Calcium complexation and cluster formation as principal modes of action of polymers used as superplasticizer in cement systems. *Cem. Concr. Res.* **2015**, *73*, 42–50. [CrossRef]
19. Lukowski, P.; Dębska, D. Effect of Polymer Addition on Performance of Portland Cement Mortar Exposed to Sulphate Attack. *Materials* **2020**, *13*, 71. [CrossRef]
20. Ramli, M.; Akhavan, T.A. Effects of polymer modification on the permeability of cement mortars under different curing conditions: A correlational study that includes pore distributions, water absorption and compressive strength. *Constr. Build. Mater.* **2012**, *28*, 561–570. [CrossRef]
21. Tian, Y.; Jin, X.Y.; Jin, N.G.; Zhao, R.; Li, Z.J.; Ma, H.Y. Research on the microstructure formation of polyacrylate latex modified mortars. *Constr. Build. Mater.* **2013**, *47*, 1381–1394. [CrossRef]
22. Liu, Q.; Lu, Z.Y.; Hu, X.S.; Chen, B.M.; Li, Z.J.; Liang, R.; Sun, G.X. A mechanical strong polymer–cement composite fabricated by in situ polymerization within the cement matrix. *J. Build. Eng.* **2021**, *42*, 103048. [CrossRef]
23. Silva, D.A.; John, V.M.; Ribeiro, J.L.D.; Roman, H.R. Pore size distribution of hydrated cement pastes modified with polymers. *Cem. Concr. Res.* **2001**, *31*, 1177–1184. [CrossRef]
24. Zhang, X.W.; Lu, C.X.; Shen, J.Y. Influence of tartaric acid on early hydration and mortar performance of Portland cement–calcium aluminate cement–anhydrite binder. *Constr. Build. Mater.* **2016**, *112*, 877–884.
25. Nguyen, D.D.; Devlin, L.P.; Koshy, P.; Sorrell, C.C. Effects of acetic acid on early hydration of Portland cement. *J. Therm. Anal. Calorim.* **2016**, *123*, 489–499. [CrossRef]
26. Zhang, Y.R.; Kong, X.M.; Lu, Z.C.; Lu, Z.B.; Zhang, Q.; Dong, B.Q.; Xing, F. Influence of triethanolamine on the hydration product of portlandite in cement paste and the mechanism. *Cem. Concr. Res.* **2016**, *87*, 64–76.
27. Huang, Y.B.; Wang, R.Z.; Zhou, J.J.; Yu, F. Effects of eva emulsion addition on magnesium phosphate cement performances. *J. Funct. Mater.* **2014**, *45*, 11071–11080.
28. Singh, N.B.; Sarvahi, R.; Singh, N.P.; Shukla, A.K. Effect of temperature on the hydration of ordinary Portland cement in the presence of a superplasticizer. *Thermochim. Acta* **1994**, *247*, 381–388. [CrossRef]
29. Morozov, Y.; Castela, A.S.; Dias, A.P.S.; Montemor, M.F. Chloride–induced corrosion behavior of reinforcing steel in spent fluid cracking catalyst modified mortars. *Cem. Concr. Res.* **2013**, *47*, 1–7. [CrossRef]

30. Mo, L.; Zhang, F.; Deng, M. Mechanical performance and microstructure of the calcium carbonate binders produced by carbonating steel slag paste under CO_2 curing. *Cem. Concr. Res.* **2016**, *88*, 217–226. [CrossRef]
31. JIE, Z.; George, W.S. Comparison of methods for arresting hydration of cement. *Cem. Concr. Res.* **2011**, *41*, 1024–1036.
32. Lu, Z.C.; Kong, X.M.; Jansen, D.; Zhang, C.Y.; Wang, J.; Pang, X.F.; Yin, J.H. Towards a further understanding of cement hydration in the presence of triethanolamine. *Cem. Concr. Res.* **2020**, *132*, 106041. [CrossRef]